nanomaterials

MDPI

Article

Influence of VO_2 Nanoparticle Morphology on the Colorimetric Assay of H_2O_2 and Glucose

Rui Tian, Jiaheng Sun, Yanfei Qi *, Boyu Zhang, Shuanli Guo and Mingming Zhao

School of Public Health, Jilin University, Changchun 130021, Jilin, China; tianrui16@mails.jlu.edu.cn (R.T.); sunjh15@mails.jlu.edu.cn (J.S.); boyu17@mails.jlu.edu.cn (B.Z.); guosl15@mails.jlu.edu.cn (S.G.); mingming17@mails.jlu.edu.cn (M.Z.)

* Correspondence: qiyanfei@jlu.edu.cn; Tel.: +86-431-8561-9441

Received: 30 September 2017; Accepted: 20 October 2017; Published: 25 October 2017

Abstract: Nanozyme-based colorimetric sensors have received considerable attention due to their unique properties. The size, shape, and surface chemistry of these nanozymes could dramatically influence their sensing behaviors. Herein, a comparative study of VO_2 nanoparticles with different morphologies (nanofibers, nanosheets, and nanorods) was conducted and applied to the sensitive colorimetric detection of H_2O_2 and glucose. The peroxidase-like activities and mechanisms of VO_2 nanoparticles were analyzed. Among the VO_2 nanoparticles, VO_2 nanofibers exhibited the best peroxidase-like activity. Finally, a comparative quantitative detections of H_2O_2 and glucose were done on fiber, sheet, and rod nanoparticles. Under the optimal reaction conditions, the lower limit of detection (LOD) of the VO_2 nanofibers, nanosheets, and nanorods for H_2O_2 are found to be 0.018, 0.266, and 0.41 mM, respectively. The VO_2 nanofibers, nanosheets, and nanorods show the linear response for H_2O_2 from 0.025–10, 0.488–62.5, and 0.488–15.625 mM, respectively. The lower limit of detection (LOD) of the VO_2 nanofibers, nanosheets, and nanorods for glucose are found to be 0.009, 0.348, and 0.437 mM, respectively. The VO_2 nanofibers, nanosheets, and nanorods show the linear response for glucose from 0.01–10, 0.625–15, and 0.625–10 mM, respectively. The proposed work will contribute to the nanozyme-based colorimetric assay.

Keywords: VO_2 nanoparticles; morphology; nanozyme; colorimetric sensor

1. Introduction

Natural enzymes with great catalytic capacity and high substrate specificity have attracted much research interest in the fields of medicine, biology, and food industry. Despite these broad developments, natural enzymes often have inherent drawbacks, such as high preparation and purification costs, low operational stability, sensitivity of catalytic activity to environmental conditions, and difficulty of recovery. These shortcomings are limited to its practical application [1]. Artificial mimic enzymes have the characteristics of high catalytic efficiency, stability, economy, and large-scale preparation which has been rapidly developed in the fields of medicine, chemical industry, food, agriculture, environmental science, and analytical chemistry [2]. Among the various artificial mimic enzymes, nanozymes as the new-generation emzyme-mimetic have attracted considerable interest since the ferroferric oxide nanomaterial has the catalytic properties similar to horseradish peroxidase (HRP) [3]. Many nanoparticles have been studied as enzyme mimetics, including ferromagnetic NPs [3–11], cerium oxide NP [12–14], metal NPs [15–23], carbon-based nanomaterials [24–28], V_2O_5 nanowires [29,30], and perovskite oxide [31,32].

Vanadium dioxide (VO_2) have received considerable attention for their redox activity and layered structures, which can serve as very good intercalation materials and smart sensors [33]. The VO_2 exists in multiple morphologies, such as fibers, nanorods, nanosheets, spheres, and hollow spheres [34,35]. The shape of the nanoparticle has attracted growing interest due to its effect on the

catalytic, optical, electronic, and magnetic properties [9,36–41]. For example, one-dimensional (1D) nanostructures—such as nanotubes, nanorods, and nanowires—exhibit higher activity and durability, compared with zero-dimensional (0D) nanostructures, due to possessing fewer lattice boundaries, fewer defect sites, and longer segments of surface crystalline planes [36]. Therefore, we focused on the effect of different morphology on the catalytic activities of VO_2 nanoparticles in order to obtain more information for their potential applications in biosensor and biocatalysts.

Herein, different morphologies VO_2 nanoparticles—including fibers, sheets, and rods—were synthesized. The catalysis activities and kinetic mechanic of various VO_2 nanoparticles were investigated upon the reaction of hydrogen peroxide with its reducing substrates 3,3′,5,5′-tetramethybenzidine (TMB). The hydrogen peroxide and glucose colorimetric sensors were developed based on VO_2 nanoparticles with different shapes. In this colorimetric assay, different analytical parameters—such as concentrations of nanoparticles, buffer solution, and pH of the analyte medium—were determined. Under optimal reaction conditions, the detection system of fiber-like VO_2 nanoparticles shows the most sensitive response to H_2O_2 and glucose than the other two VO_2 nanoparticles.

2. Results and Discussions

2.1. Characterization of VO_2 Nanoparticles

The structural characterizations of the VO_2 nanoparticles were done by transmission electron microscopy (TEM) and X-ray powder Diffraction (XRD). TEM images indicate the VO_2 nanoparticles of different morphology, fibers, rods, and sheets (Figure 1). The formation of VO_2 nanoparticles is confirmed from the X-ray diffraction pattern (Figure 2). The VO_2 nanoparticles with fiber, sheet, and rod shapes have the same crystal structures as those reported in the literature [34,35], and are monoclinic VO_2 (Joint Committee on Powder Diffraction Standards card No. 31-1438 and No. 65-7960: see Figure 2).

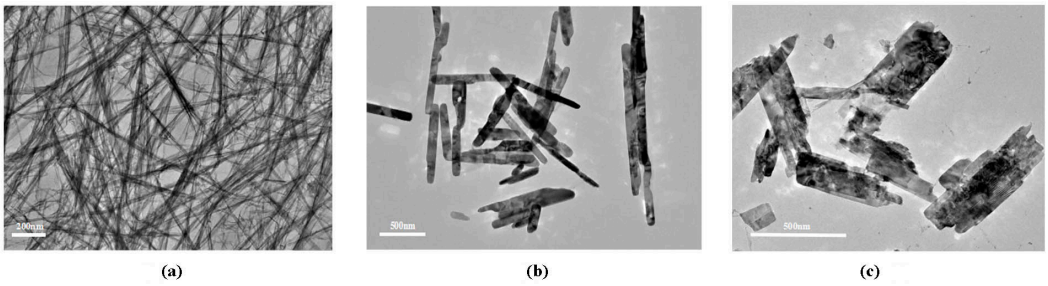

Figure 1. TEM images of VO_2 nanoparticles. (**a**) VO_2 nanofibers (**b**) VO_2 nanosheets (**c**) VO_2 nanorods.

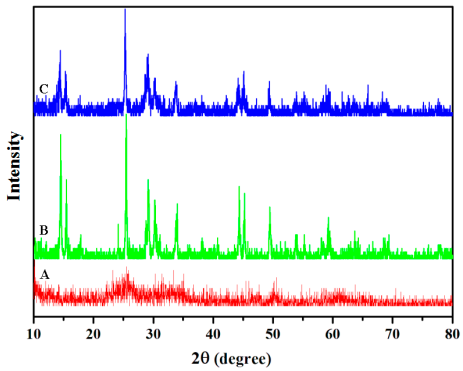

Figure 2. XRD patterns of VO_2 nanoparticles. (**A**) VO_2 nanofiber; (**B**) VO_2 nanosheets; (**C**) VO_2 nanorods.

2.2. Principle

In pH 4 citrate buffer solution at room temperature, VO_2 nanoparticles with different morphologies catalyzed the oxidation of a peroxidase substrate 3,3′,5,5′-tetramethylbenzidine (TMB) in the presence of H_2O_2 to obtain the TMB oxidized product with blue color. As shown in Figure 3, when various VO_2 nanoparticles were added into the TMB/H_2O_2 solution, the strong absorption peaks were obtained at 656 nm. However, there were no strong absorption peaks when the solution did not contain H_2O_2 or VO_2 nanoparticles. The absorbance becomes stronger due to more TMB being oxidized with the increasing of the concentration of H_2O_2. The absorbance also showed a linear trend depending on the concentration of H_2O_2.

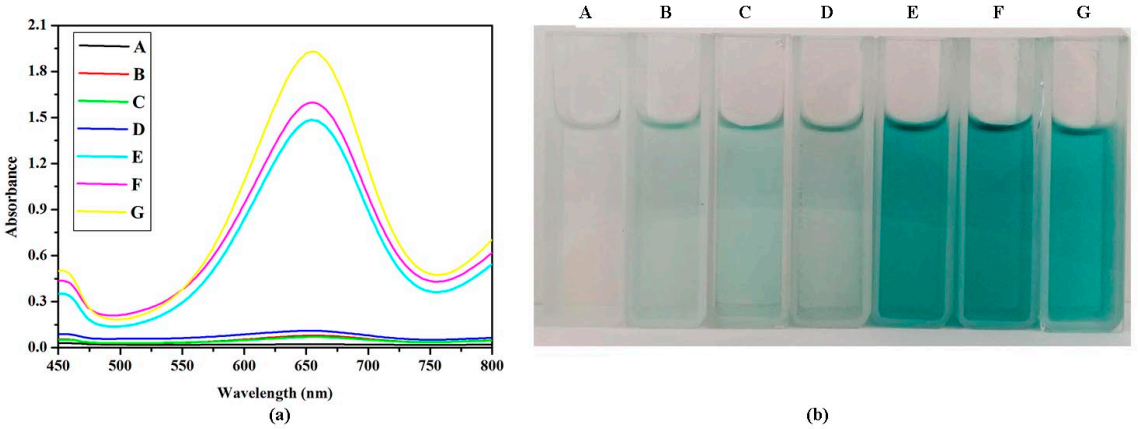

Figure 3. UV-Visible absorption spectra (**a**) and color changes (**b**) of different reaction systems. ((**A**) TMB + H_2O_2, (**B**) TMB + VO_2 nanorod, (**C**) TMB + VO_2 nanosheet, (**D**) TMB + VO_2 nanofiber, (**E**) TMB + VO_2 nanorod + H_2O_2, (**F**) TMB + VO_2 nanosheet + H_2O_2, (**G**) TMB +VO_2 nanofiber + H_2O_2).

2.3. Effect of pH

The effect of pH value (pH 3.0–8.0) on absorption value with TMB was investigated in the citrate buffer system, as shown in Figure 4. Each of the VO_2 nanofibers, nanosheets, and nanorods of the system reached their maximum peaks when the pH value was 4.0. Therefore, pH 4.0 was selected to detect H_2O_2 and glucose with various VO_2 nanoparticles.

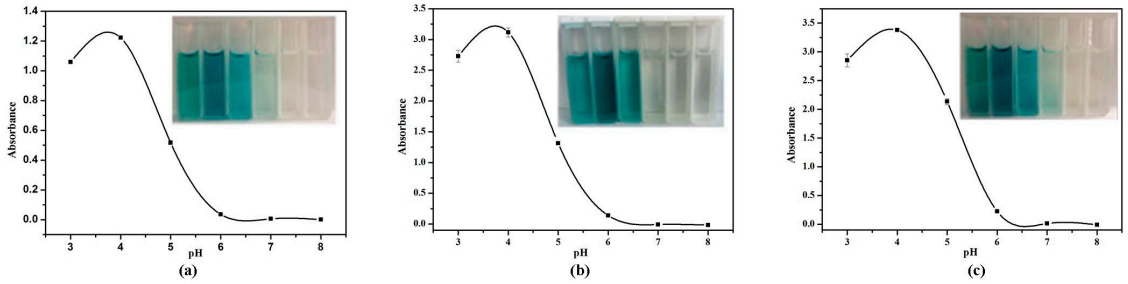

Figure 4. The effect of pH on absorption value with TMB and color changes. (**a**) VO_2 nanofibers; (**b**) VO_2 nanosheets; (**c**) VO_2 nanorods. The error bars represent the standard deviation of three measurements.

2.4. Effect of Buffers

The effect of buffers on absorption value of TMB oxide product was examined. The time response curves of TMB with H_2O_2 catalyzed by VO_2 with different morphologies, in pH 4.0, 0.2 M acetate, phosphate, and citrate buffers. The results were shown in Figure 5. Up to 300 s, the VO_2 nanoparticles were more active in the citrate buffer solution. Thus, the citrate buffer solution (pH = 4.0, 0.2 M), was chosen as the optimal reaction solution for the H_2O_2 and glucose colorimetric assay.

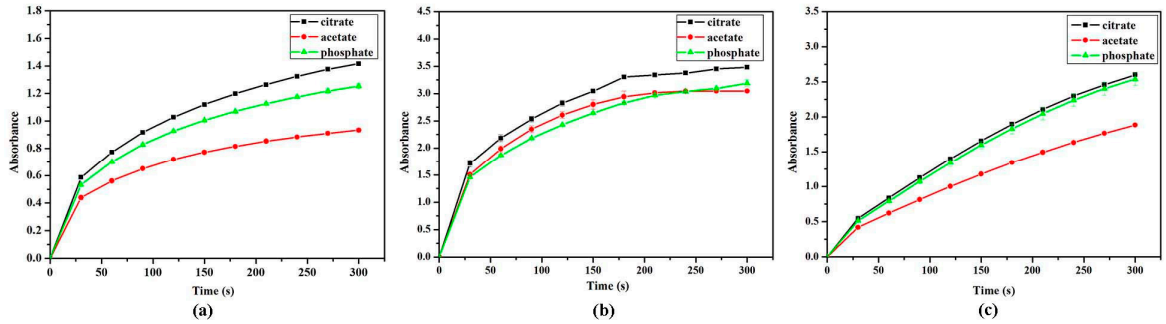

Figure 5. The effect of buffer solution on absorption value with TMB. (**a**) VO_2 nanofibers; (**b**) VO_2 nanosheets; (**c**) VO_2 nanorods. The error bars represent the standard deviation of three measurements.

2.5. Effect of VO_2 Nanoparticle Morphologies and Concentrations

As shown in Figure 6, the absorption values at OD_{656nm} of TMB oxide product increased gradually with the concentration of VO_2 nanoparticles. The system reached its maximum absorption value when the concentrations of VO_2 nanofibers, nanosheets, and nanorods were 10, 10, and 2 mM, respectively. The results show that the catalytic activity of VO_2 nanofibers is stronger than the other two, shown in the Figure 6.

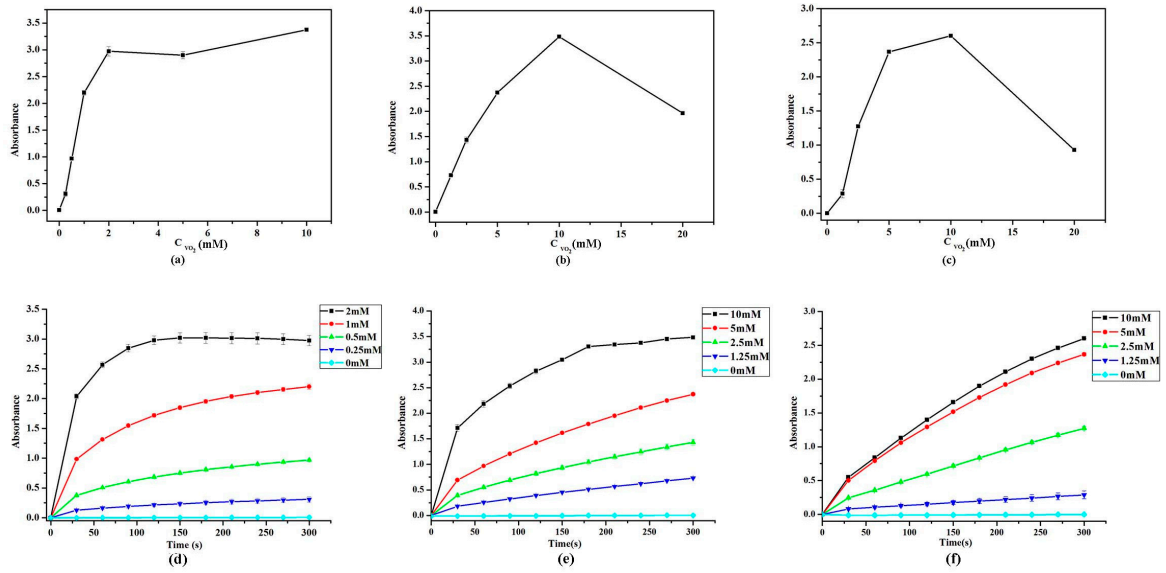

Figure 6. The effect of VO_2 nanofibers (**a**,**d**); VO_2 nanosheets (**b**,**e**); and VO_2 nanorods (**c**,**f**) concentrations on absorption value with TMB in pH 4.0 citrate buffer solution. The error bars represent the standard deviation of three measurements.

2.6. Steady-State Kinetic Assay

For further understanding the influence of particle morphology on the catalytic mechanism of VO_2 nanoparticles, the steady-state kinetic assay for VO_2 nanoparticles were determined in detail. As shown in Figure 7, the typical Michaelis-Menten curve were obtained for VO_2 nanozymes. Michaelis-Menten constant (K_M) and maximum initial velocity (V_{max}) were known from Michaelis-Menten curve use a Lineweaver-Burk plot. A comparison of the kinetic parameters of VO_2 nanozymes, V_2O_5 nanozymes, Fe_3O_4 magnetic nanoparticle (MNP_S), and HRP was given in Table 1. The K_M of VO_2 nanofibers, nanosheets, and nanorods with TMB were 0.518, 0.111, and 0.801 mM, respectively. The V_{max} of VO_2 nanofibers, nanosheets, and nanorods with TMB were 9.3×10^{-5}, 1.68×10^{-4}, and 3.99×10^{-4} $M \cdot s^{-1}$, respectively. The K_M of VO_2 nanofibers, nanosheets, and nanorods with H_2O_2 were 1.043, 2.924,

and 6.469 mM. The V_{max} of VO_2 nanofibers, nanosheets, and nanorods with H_2O_2 were 4.66×10^{-4}, 9.73×10^{-4}, and 1.46×10^{-3} $M \cdot s^{-1}$, respectively. The K_M values shows that VO_2 nanosheets with TMB as the substrate was apparently lower than VO_2 nanofibers, VO_2 nanorods, V_2O_5 nanozymes, Fe_3O_4 MNP_S, and HRP. It shows that the VO_2 nanosheets have a higher affinity to TMB compared with VO_2 nanofibers, VO_2 nanorods, Fe_3O_4 MNP_S, and HRP. Which means that a lower TMB concentration was required to reach the maximal activity for VO_2 nanosheets. The apparent K_M values of VO_2 nanofibers with H_2O_2 as the substrate was apparently lower than VO_2 nanorods, VO_2 nanosheets, Fe_3O_4 MNP_S, and HRP. It shows that the VO_2 nanofibers have a higher affinity for H_2O_2 compared with VO_2 nanosheets, VO_2 nanorods, Fe_3O_4 MNP_S, and HRP. That means a lower H_2O_2 concentration was required to reach the maximal activity for VO_2 nanofibers.

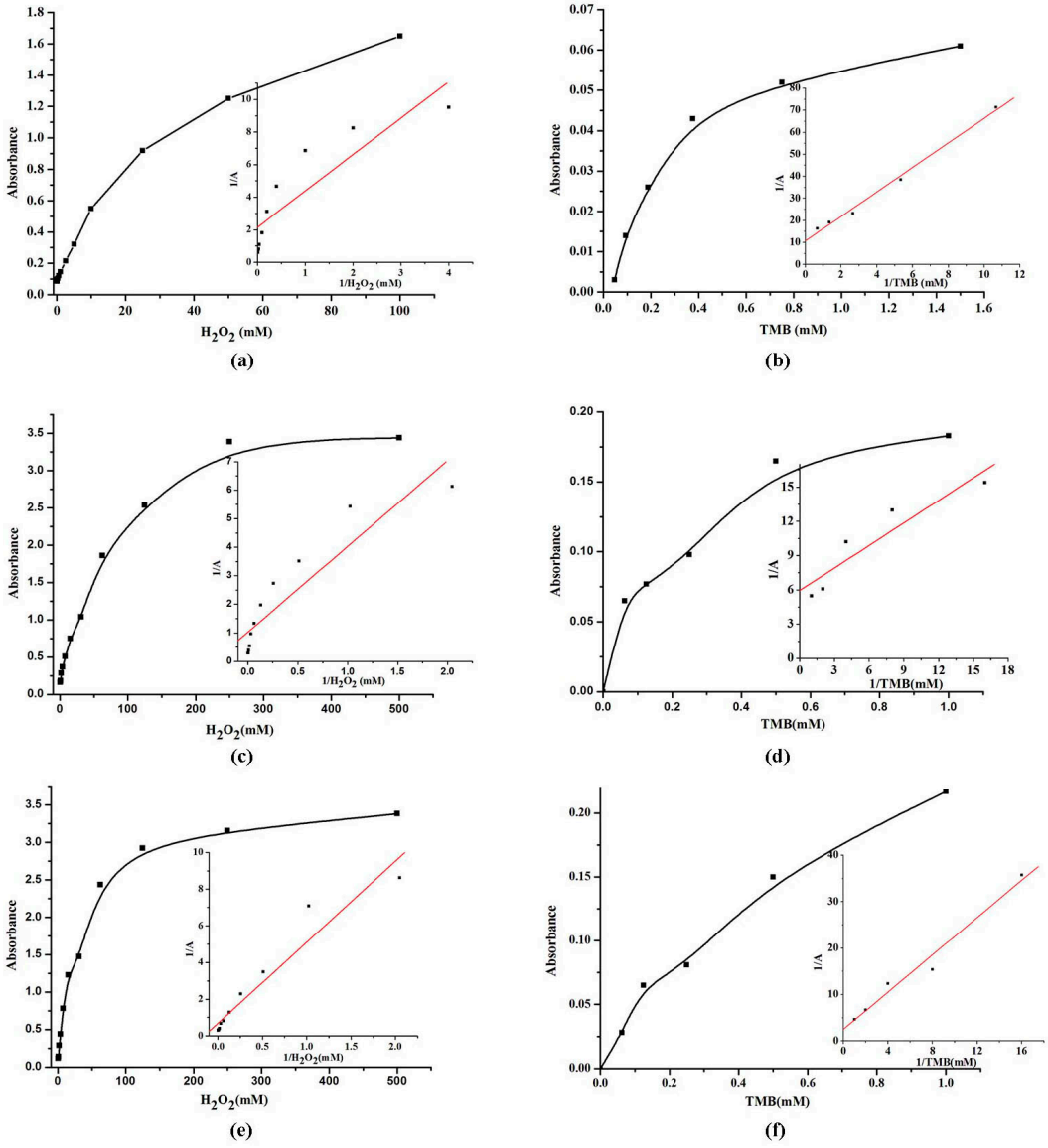

Figure 7. The steady-state kinetic assay and catalytic mechanism of VO_2 nanofibers (**a**,**b**); VO_2 nanosheets (**c**,**d**); and VO_2 nanorods (**e**,**f**) as peroxidase mimics. Conditions: pH, 4.0 (0.2 M citrate buffer); temperature, 25 °C; incubation time, 5 min.

Table 1. Comparison of the K_M and V_{max} of VO_2 nanozymes, V_2O_5 nanozymes, Fe_3O_4 MNP_S, and HRP, respectively.

Nanozymes	Substrate	K_M (mM)	V_{max} ($M \cdot S^{-1}$)
VO_2 nanofibers	TMB	0.518	9.3×10^{-5}
VO_2 nanofibers	H_2O_2	1.043	4.66×10^{-4}
VO_2 nanosheets	TMB	0.111	1.68×10^{-4}
VO_2 nanosheets	H_2O_2	2.924	9.73×10^{-4}
VO_2 nanorods	TMB	0.801	3.99×10^{-4}
VO_2 nanorods	H_2O_2	6.469	1.46×10^{-3}
V_2O_5 nanozymes	TMB	0.738	1.85×10^{-5}
V_2O_5 nanozymes	H_2O_2	0.232	1.29×10^{-5}
Fe_3O_4 MNPS	TMB	0.434	10.00×10^{-8}
Fe_3O_4 MNPS	H_2O_2	154	9.78×10^{-8}
HRP	TMB	0.434	1.24×10^{-8}
HRP	H_2O_2	3.70	2.46×10^{-8}

2.7. Calibration Curve for H_2O_2 and Glucose Detection

Under the optimal conditions (pH 4.0 citrate buffer, the concentrations of VO_2 nanofibers, nanosheets and nanorods were 2, 10, and 10mM, respectively.) the calibration curves of H_2O_2 were obtained with VO_2 nanoparticles different morphologies (Figure 8). The correlation between the absorbance values and H_2O_2 concentration are linear over the range of 0–100 mM (nanofibers), 0–500 mM (nanosheets) and 0–500 mM (nanorods) with correlation coefficients 0.99981, 0.99364, and 0.99222, respectively. The lower limit of detection (LOD) of the VO_2 nanofibers, nanosheets, and nanorods for H_2O_2 are found to be 0.018, 0.266, and 0.41 mM, respectively.

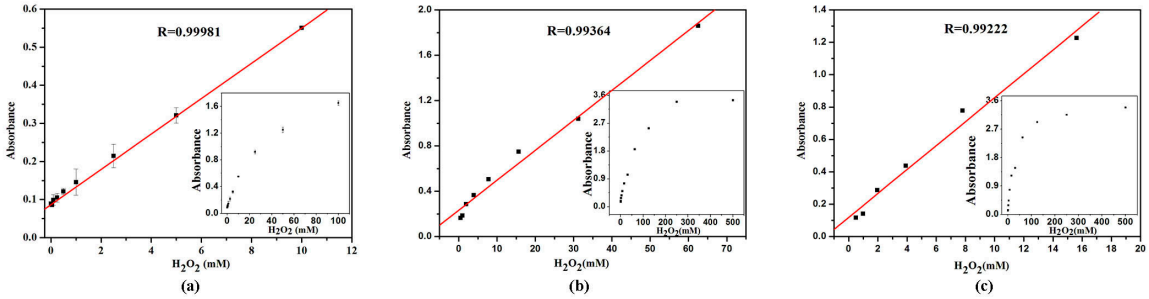

Figure 8. A dose-response curve depending of the absorbance at 656 nm in the presence of different concentrations of H_2O_2. (**a**) VO_2 nanofibers; (**b**) VO_2 nanosheets; (**c**) VO_2 nanorods. Error bars represent the standard deviation of three measurements. Conditions: pH, 4.0 (0.2 M citrate buffer); temperature, 25 °C; incubation time, 5 min.

As glucose oxidase (GOx) can catalyze the oxidation of glucose and produce H_2O_2, the absorption value with TMB was changing by H_2O_2 in presence of VO_2 nanoparticles. Because the GOx would be denatured in pH 4.0 buffer, the glucose detection was produced in two steps: first, H_2O_2 was induced by GOx oxidation of glucose and then the reaction solutions were detected by TMB/different VO_2 nanoparticles system. As shown in Figure 9, the absorbtion increases gradually with the increasing of glucose concentration. The correlation between the absorbance at 656 nm and glucose concentration are linear over the range of 0–30 mM (nanofibers), 0–40 mM (nanosheets) and 0–40 mM (nanorods) with the correlation coefficient of 0.98557, 0.98919, and 0.99502, respectively. The lower limit of detection (LOD) of the VO_2 nanofibers, nanosheets, and nanorods for glucose are found to be 0.009, 0.348, and 0.437 mM, respectively.

The VO_2 nanofibers showed the highest peroxidase activity in the H_2O_2 and glucose colorimetric assay, followed by VO_2 nanosheets, and finally VO_2 nanorods. Additionally, it was reported that

the specific surface area of VO_2 nanoparticles greatly influences their catalytic activities. The specific surface area of VO_2 nanofibers (185 to 122 m^2 g^{-1}) [34] is also much larger than that of other VO_2 micro/nanoparticles, such as hollow microspheres (22.3 m^2 g^{-1}), nanowires (12.3 m^2 g^{-1}) [42], nanobelts (18.6 m^2 g^{-1}) [43], nanorods (42 m^2 g^{-1}) [44], VO_2 mesocrystals (28.4 m^2 g^{-1}) [45], mesoporous VO_2 nanowires (46.7 m^2 g^{-1}) [46], and 3D GO-VO_2 nanosheet flowers (71.6 m^2 g^{-1}) [47]. Therefore, the VO_2 nanofibers demonstrated the most sensitive response during the H_2O_2 and glucose sensing. By comparing with other nanozymes to further understanding the catalytic activity of VO_2 nanozymes as peroxidase mimetics, as shown in Table 2, the VO_2 nanofibers have a wider linear range.

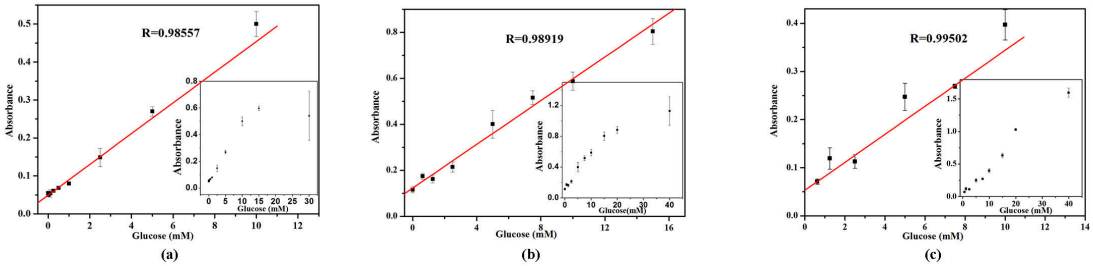

Figure 9. A dose-response curve depending of the absorbance at 656 nm in the presence of different concentrations of glucose. (**a**) VO_2 nanofibers; (**b**) VO_2 nanosheets; (**c**) VO_2 nanorods, in which error bars represent the standard deviation of three measurements. Conditions: pH, 4.0 (0.2 M citrate buffer); temperature, 25 °C; incubation time, 5 min.

Table 2. Comparison of different nanozymes for the detection of H_2O_2.

Nanozymes	Linear Range	Limit of Detection	Reference
Fe_3O_4 MNP_S	1–100 μM	0.5 μM	[48]
HRP	1–60 μM	1 μM	[49]
Pt-DNA complexes	0.979–17.6 mM	0.392 mM	[50]
V_2O_5 nanozymes	1–500 μM	1 μM	[30]
VO_2 nanofibers	0.025–10 mM	0.018 mM	This work
VO_2 nanosheets	0.488–62.5 mM	0.266 mM	This work
VO_2 nanorods	0.488–15.6 mM	0.41 mM	This work

3. Materials and Methods

3.1. Chemicals and Materials

All the chemicals used were of analysis grade without further purification. 3,3′,5,5′-Tetramethylbenzidine (TMB) was obtained from Tokyo Chemical Industry Co., Ltd. (Tokyo, Japan). Glucose oxidase (GOx) was obtained from Aladdin Reagent Co., Ltd. (Shanghai, China). V_2O_5, oxalic acid, methanol, glucose, hydrogen peroxide (H_2O_2, 30%), etc., were purchased from Beijing Chemical Works (Beijing, China). The water used in the experiments was purified.

3.2. Synthesis of VO_2 Nanoparticles

The synthesis of VO_2 nanofiber contains two steps: synthesis of VO_2 hollow sphere and the supernatant collecting and drying. According to the literature procedure [35] synthesis of VO_2 hollow sphere, with minor adjustment. Briefly, V_2O_5 and oxalic acid (the ratio of molar is 1:3) were first dissolved in 7 mL distilled water and stirred for 10 min at room temperature. Then the 23 mL methanol was added in the solution and stirred for another 10 min. The mix solution was transferred to a Teflon-lined autoclave with stainless steel, and heated at 200 °C for 24 h. The sample was cooled down naturally. The black precipitates were filtered off and washed with distilled water and ethanol, and then dried at 80 °C overnight, and finally the VO_2 hollow spheres were dissolved, the supernatant

was collected and dried. Similar procedures were adopted to prepare nanorods and nanosheets: when the water content is 10 mL, the product is nanorods, and when the solution is completely water, the product is just nanosheets (with water and methanol measures maintained at 30 mL).

3.3. Physical Characterization

The morphology and size of the VO_2 nanoparticles were acquired using a transmission electron microscopy (TEM) by JEM-1011 transmission electron microscopy (JEOL, Tokyo, Japan) with a working voltage at 100 kV. The X-ray powder diffraction method was carried out in a D/max-rα power diffractometer (Rigaku, Tokyo, Japan) using Cu-Kα monochromatic radiation (λ = 1.5418 Å).

3.4. H_2O_2 Detection Using VO_2 Nanoparticles as Peroxidase Mimetics

To discover the peroxidase-like character of VO_2 nanoparticles, the experiments were performed as follows: 60 μL VO_2 nanoparticles solution (the concentrations of nanofibers, nanosheets, and nanorods are 2, 10, and 10 mM, respectively) in a reaction volume of 2400 μL citrate buffer solution (pH = 4.0) and 480 μL TMB solution (1.5 mM in ethanol), followed by the addition of 60 μL H_2O_2 (30%). The mixed solution was reacted for 5 min at room temperature. Then used for the UV-Vis spectrophotometer (Metash Instruments Inc., Shanghai, China) record the spectra at 656 nm for TMB.

To investigate the influence of buffer solution on the VO_2 nanoparticle characteristics, the pH—ranging from 3.0 to 8.0 of the buffer solution—was examined, under conditions identical to these used above.

To investigate the influence of different reaction buffers on the VO_2 nanoparticles characteristics, catalytic reactions incubated in difference buffer solution—including citrate, phosphate, and acetate—were examined, under conditions identical to these used in above. For a blank, only substrate solution was used. All experiments were conducted at room temperature (25 °C).

3.5. Glucose Detection Using VO_2 Nanoparticles

Glucose detection was examined as follows: (a) 200 μL of GOx (1 mg/mL) and 200 μL of glucose of different concentrations in 400 μL of phosphate buffered saline (PBS, pH = 7.0) were incubated at 37 °C for 60 min; (b) 400 μL of TMB (1.5 mM in ethanol) and 50 μL of VO_2 nanoparticles solution (the concentrations of nanofibers, nanosheets, and nanorods are 2, 10, and 10 mM, respectively) in 1750 μL of citrate buffer solution (pH = 4.0) were added into the above glucose reaction solution; (c) The mixed solutions with different concentrations of glucose were incubated for 5 min; the (d) the UV-Vis spectrophotometer was used to record the spectra.

4. Conclusions

VO_2 nanoparticles with different structures—nanofibers, nanosheets, and nanorods—have been successfully fabricated and show peroxidase-like activities. The catalytic behaviors of VO_2 nanoparticles show Michaelis-Menten kinetics and good affinity to both H_2O_2 and TMB. The VO_2 nanoparticle-based colorimetric assay provides fast, sensitive, and low-cost H_2O_2 and glucose sensors. Compared with VO_2 nanorods and VO_2 nanosheets, the VO_2 nanofibers demonstrated the most sensitive response during the H_2O_2 and glucose sensing. This investigation is significant for vanadium-based nanozyme application in biosensor and biocatalysis.

Acknowledgments: This work was financially supported by NSFC (81402719) and Norman Bethune Program of Jilin University (2015228).

Author Contributions: Yanfei Qi conceived and designed the experiments; Rui Tian performed the experiments and analyzed the data; Yanfei Qi contributed reagents, materials, and analysis tools; Boyu Zhang, Yanfei Qi, Rui Tian, Shuanli Guo, Jiaheng Sun, and Mingming Zhao wrote the paper.

Conflicts of Interest: The authors declare no conflict of interest. The founding sponsors had no role in the design of the study; in the collection, analyses, or interpretation of data; in the writing of the manuscript, or in the decision to publish the results.

References

1. Huang, Y.Y.; Ran, X.; Lin, Y.H.; Ren, J.S.; Qu, X.G. Self-assembly of an organic-inorganic hybrid nanoflower as an efficient biomimetic catalyst for self-activated tandem reactions. *Chem. Commun.* **2015**, *51*, 4386–4389. [CrossRef] [PubMed]
2. Liang, A.H.; Wang, X.L.; Wen, G.Q.; Jiang, Z.L. A sensitive and selective Victoria blue 4R SERS molecular probe for sodium lauryl sulfate in AuNP/AgCl sol substrate. *Sens. Actuators B* **2017**, *244*, 275–281. [CrossRef]
3. Gao, L.Z.; Zhuang, J.; Nie, L.; Zhang, J.B.; Zhang, Y.; Gu, N.; Wang, T.H.; Feng, J.; Yang, D.L.; Perrett, S.; et al. Intrinsic peroxidase-like activity of ferromagnetic nanoparticles. *Nat. Nanotechnol.* **2007**, *2*, 577–583. [CrossRef] [PubMed]
4. Srikanth Vallabani, N.V.; Karakoti, A.S.; Singh, S. ATP-mediated intrinsic peroxidase-like activity of Fe_3O_4-based nanozyme: One step detection of blood glucose at physiological pH. *Colloids Surfaces B* **2017**, *153*, 52–60. [CrossRef] [PubMed]
5. Wei, H.; Wang, E. Fe_3O_4 Magnetic Nanoparticles as Peroxidase Mimetics and Their Applications in H_2O_2 and Glucose Detection. *Anal. Chem.* **2008**, *80*, 2250–2254. [CrossRef] [PubMed]
6. Zhang, X.Q.; Gong, S.W.; Zhang, Y.; Yang, T.; Wang, C.Y.; Gu, N. Prussian blue modified iron oxide magnetic nanoparticles and their high peroxidase-like activity. *Mater. Chem.* **2010**, *20*, 5110–5116. [CrossRef]
7. Shi, W.B.; Zhang, X.D.; He, S.H.; Huang, Y.M. $CoFe_2O_4$ magnetic nanoparticles as a peroxidase mimic mediated chemiluminescence for hydrogen peroxide and glucose. *Chem. Commun.* **2011**, *47*, 10785–10787. [CrossRef] [PubMed]
8. Yu, F.Q.; Huang, Y.Z.; Cole, A.J.; Yang, V.C. The artificial peroxidase activity of magnetic iron oxide nanoparticles and its application to glucose detection. *Biomaterials* **2009**, *30*, 4716–4722. [CrossRef] [PubMed]
9. Liu, S.H.; Lu, F.; Xing, R.M.; Zhu, J.J. Structural Effects of Fe_3O_4 Nanocrystals on Peroxidase-Like Activity. *Chem. Eur. J.* **2011**, *17*, 620–625. [CrossRef] [PubMed]
10. Park, K.S.; Kim, M.I.; Cho, D.Y.; Park, H.G. Label-Free Colorimetric Detection of Nucleic Acids Based on Target-Induced Shielding Against the Peroxidase-Mimicking Activity of Magnetic Nanoparticles. *Small* **2011**, *7*, 1521–1525. [CrossRef] [PubMed]
11. Wang, N.; Zhu, L.H.; Wang, M.Q.; Wang, D.L.; Tang, H.Q. Sono-enhanced degradation of dye pollutants with the use of H_2O_2 activated by Fe_3O_4 magnetic nanoparticles as peroxidase mimetic. *Ultrason. Sonochem.* **2010**, *17*, 78–83. [CrossRef] [PubMed]
12. Korsvik, C.; Patil, S.; Seal, S.; Self, W.T. Superoxide dismutase mimetic properties exhibited by vacancy engineered ceria nanoparticles. *Chem. Commun.* **2007**, *14*, 1056–1058. [CrossRef] [PubMed]
13. Asati, A.; Santra, S.; Kaittanis, C.; Nath, S.; Perez, J.M. Oxidase-Like Activity of Polymer-Coated Cerium Oxide Nanoparticles. *Angew. Chem. Int. Ed.* **2009**, *48*, 2308–2312. [CrossRef] [PubMed]
14. Pirmohamed, T.; Dowding, J.M.; Singh, S.; Wasserman, B.; Heckert, E.; Karakoti, A.S.; King, J.E.; Seal, S.S.; Self, W.T. Nanoceria exhibit redox state-dependent catalase mimetic activity. *Chem. Commun.* **2010**, *46*, 2736–2738. [CrossRef] [PubMed]
15. He, W.W.; Wu, X.C.; Liu, J.B.; Hu, X.N.; Zhang, K.; Hou, S.; Zhou, W.Y.; Xie, S.S. Design of AgM Bimetallic Alloy Nanostructures (M = Au, Pd, Pt) with Tunable Morphology and Peroxidase-Like Activity. *Chem. Mater.* **2010**, *22*, 2988–2994. [CrossRef]
16. Jv, Y.; Li, B.X.; Cao, R. Positively-charged gold nanoparticles as peroxidiase mimic and their application in hydrogen peroxide and glucose detection. *Chem. Commun.* **2010**, *46*, 8017–8019. [CrossRef] [PubMed]
17. Fan, J.; Yin, J.J.; Ning, B.; Wu, X.C.; Hu, Y.; Ferrari, M.; Anderson, G.J.; Wei, J.Y.; Zhao, Y.L.; Nie, G.J. Direct evidence for catalase and peroxidase activities of ferritine—Platinum nanoparticles. *Biomaterials* **2011**, *32*, 1611–1618. [CrossRef] [PubMed]
18. He, W.W.; Liu, Y.; Yuan, J.S.; Yin, J.J.; Wu, X.C.; Hu, X.N.; Zhang, K.; Liu, J.B.; Chen, C.Y.; Ji, Y.L.; et al. Au@Pt nanostructures as oxidase and peroxidase mimetics for use in immunoassays. *Biomaterials* **2011**, *32*, 1139–1147. [CrossRef] [PubMed]
19. Liu, J.B.; Hu, X.N.; Hou, S.; Wen, T.; Liu, W.Q.; Zhu, X.; Wu, X.C. Screening of inhibitors for oxidase mimics of Au@Pt nanorods by catalytic oxidation of OPD. *Chem. Commun.* **2011**, *47*, 10981–10983. [CrossRef] [PubMed]
20. Wang, X.X.; Wu, Q.; Shan, Z.; Huang, Q.M. BSA-stabilized Au clusters as peroxidase mimetics for use in xanthine detection. *Biosens. Bioelectron.* **2011**, *26*, 3614–3619. [CrossRef] [PubMed]

21. Jiang, H.; Chen, Z.H.; Cao, H.Y.; Huang, Y.M. Peroxidase-like activity of chitosan stabilized silver nanoparticles for visual and colorimetric detection of glucose. *Analyst* **2012**, *137*, 5560–5564. [CrossRef] [PubMed]
22. Wang, S.S.; Chen, Z.P.; Choo, J.; Chen, L.X. Naked-eye sensitive ELISA-like assay based on gold-enhanced peroxidase-like immunogold activity. *Anal. Bioanal. Chem.* **2016**, *408*, 1015–1022. [CrossRef] [PubMed]
23. Chen, W.; Chen, J.; Liu, A.L.; Wang, L.M.; Li, G.W.; Lin, X.H. Peroxidase-like activity of cupric oxide nanoparticle. *Chem. Cat. Chem.* **2011**, *3*, 1151–1154. [CrossRef]
24. Song, Y.J.; Qu, K.G.; Zhao, C.; Ren, J.S.; Qu, X.G. Graphene Oxide: Intrinsic Peroxidase Catalytic Activity and Its Application to Glucose Detection. *Adv. Mater.* **2010**, *22*, 2206–2210. [CrossRef] [PubMed]
25. Song, Y.J.; Wang, X.H.; Zhao, C.; Qu, K.G.; Ren, J.S.; Qu, X.G. Label-Free Colorimetric Detection of Single Nucleotide Polymorphism by Using Single-Walled Carbon Nanotube Intrinsic Peroxidase-Like Activity. *Chem. Eur. J.* **2010**, *16*, 3617–3621. [CrossRef] [PubMed]
26. Shi, W.B.; Wang, Q.L.; Long, Y.J.; Cheng, Z.L.; Chen, S.H.; Zheng, H.Z.; Huang, Y.M. Carbon nanodots as peroxidase mimetics and their applications to glucose detection. *Chem. Commun.* **2011**, *47*, 6695–6697. [CrossRef] [PubMed]
27. Song, Y.J.; Chen, Y.; Feng, L.Y.; Ren, J.S.; Qu, X.G. Selective and quantitative cancer cell detection using target-directed functionalized graphene and its synergetic peroxidase-like activity. *Chem. Commun.* **2011**, *47*, 4436–4438. [CrossRef] [PubMed]
28. Wang, X.H.; Qu, K.G.; Xu, B.L.; Ren, J.S.; Qu, X.G. Multicolor Luminescent Carbon Nanoparticles: Synthesis, Supramolecular Assembly with Porphyrin, Intrinsic Peroxidase-Like Catalytic Activity and Applications. *Nano Res.* **2011**, *4*, 908–920. [CrossRef]
29. Andre, R.; Natalio, F.; Humanes, M.; Leppin, J.; Heinze, K.; Wever, R.; Schroder, H.C.; Muller, W.E.G.; Tremel, W. V_2O_5 Nanowires with an Intrinsic Peroxidase-Like Activity. *Adv. Funct. Mater.* **2011**, *21*, 501–509. [CrossRef]
30. Sun, J.H.; Li, C.Y.; Qi, Y.F.; Guo, S.L.; Liang, X. Optimizing Colorimetric Assay Based on V_2O_5 Nanozymes for Sensitive Detection of H_2O_2 and Glucose. *Sensors* **2016**, *16*, 584. [CrossRef] [PubMed]
31. Xiao, P.; Hong, J.P.; Wang, T.; Xu, X.L.; Yuan, Y.H.; Li, J.L. Oxidative Degradation of Organic Dyes Over Supported Perovskite Oxide $LaFeO_3$/SBA-15 Under Ambient Conditions. *Springer* **2013**, *143*, 887–894. [CrossRef]
32. Li, Z.Y.; Zhou, Y.; Qi, H.; Pan, Q.W.; Zhang, Z.; Shi, N.N.; Lu, M.; Stein, A.C.; Li, Y.; Ramanathan, S.; et al. Correlated Perovskites as a New Platform for Super-Broadband-Tunable Photonics. *Adv. Mater.* **2016**, *28*, 9117–9125. [CrossRef] [PubMed]
33. Nie, G.D.; Zhang, L.; Lei, J.Y.; Yang, L.; Zhang, Z.; Lu, X.F.; Wang, C. Monocrystalline VO_2 (B) nanobelts: Large-scale synthesis, intrinsic peroxidase-like activity and application in biosensing. *J. Mater. Chem. A* **2014**, *2*, 2910–2914. [CrossRef]
34. Baudrin, E.; Sudant, G.; Larcher, D.; Dunn, B.; Tarascon, J.M. Preparation of Nanotextured VO_2[B] from Vanadium Oxide Aerogels. *Chem. Mater.* **2006**, *18*, 4369–4374. [CrossRef]
35. Pan, J.; Zhong, L.; Li, M.; Luo, Y.Y.; Li, G.H. Microwave-Assisted Solvothermal Synthesis of VO_2 Hollow Spheres and Their Conversion into V_2O_5 Hollow Spheres with Improved Lithium Storage Capability. *Chem. Eur. J.* **2016**, *22*, 1461–1466. [CrossRef] [PubMed]
36. Xiao, Q.F.; Cai, M.; Balogh, M.P.; Tessema, M.M.; Lu, Y.F. Symmetric Growth of Pt Ultrathin Nanowires from Dumbbell Nuclei for Use as Oxygen Reduction Catalysts. *Nano Res.* **2012**, *5*, 145–151. [CrossRef]
37. Han, X.G.; Jin, M.S.; Xie, S.F.; Kuang, Q.; Jiang, Z.Y.; Jiang, Y.Q.; Xie, Z.X.; Zheng, L.S. Synthesis of Tin Dioxide Octahedral Nanoparticles with Exposed High-Energy {221} Facets and Enhanced Gas-Sensing Properties. *Angew. Chem. Int. Ed.* **2009**, *48*, 9180–9183. [CrossRef] [PubMed]
38. Yang, H.G.; Liu, G.; Qiao, S.Z.; Sun, C.H.; Jin, Y.G.; Smith, S.C.; Zou, J.; Cheng, H.M.; Lu, G.Q. Solvothermal Synthesis and Photoreactivity of Anatase TiO_2 Nanosheets with Dominant {001} Facets. *J. Am. Chem. Soc.* **2009**, *131*, 4078–4083. [CrossRef] [PubMed]
39. Fan, D.B.; Thomas, P.J.; O'Brien, P. Pyramidal Lead Sulfide Crystallites with High Energy {113} Facets. *J. Am. Chem. Soc.* **2008**, *130*, 10892–10894. [CrossRef] [PubMed]
40. Tao, A.R.; Habas, S.; Yang, P.D. Shape control of colloidal metal nanocrystals. *Small* **2008**, *4*, 310–325. [CrossRef]

41. Zhou, Y.; Park, J.W.; Shi, J.; Chhowalla, M.; Park, H.; Weitz, D.A.; Ramanathan, S. Control of Emergent Properties at a Correlated Oxide Interface with Graphene. *Nano Lett.* **2015**, *15*, 1627–1634. [CrossRef] [PubMed]
42. Niu, C.J.; Meng, J.S.; Han, C.H.; Zhao, K.N.; Yan, M.Y.; Mai, L.Q. VO_2 Nanowires Assembled into Hollow Microspheres for High-Rate and Long-Life Lithium Batteries. *Nano Lett.* **2014**, *14*, 2873–2878. [CrossRef] [PubMed]
43. Mai, L.Q.; Wei, Q.L.; An, Q.Y.; Tian, X.C.; Zhao, Y.L.; Xu, X.; Xu, L.; Chang, L.; Zhang, Q.J. Nanoscroll Buffered Hybrid Nanostructural VO_2 (B) Cathodes for High-Rate and Long-Life Lithium Storage. *Adv. Mater.* **2013**, *25*, 2969–2973. [CrossRef] [PubMed]
44. Quites, F.J.; Pastore, H.O. Hydrothermal synthesis of nanocrystalline VO_2 from poly (diallyldimethylammonium) chloride and V_2O_5. *Mater. Res. Bull.* **2010**, *45*, 892–896. [CrossRef]
45. Uchaker, E.; Gu, M.; Zhou, N.; Li, Y.W.; Wang, C.M.; Cao, G.Z. Enhanced Intercalation Dynamics and Stability of Engineered Micro/Nano-Structured Electrode Materials: Vanadium Oxide Mesocrystals. *Small* **2013**, *9*, 3880–3886. [CrossRef] [PubMed]
46. Zhang, L.; Zhao, K.N.; Xu, W.W.; Meng, J.S.; He, L.; An, Q.Y.; Xu, X.; Luo, Y.Z.; Zhao, T.W.; Mai, L.Q. Mesoporous VO_2 nanowires with excellent cycling stability and enhanced rate capability for lithium batteries. *RSC Adv.* **2014**, *4*, 33332–33337. [CrossRef]
47. Nethravathi, C.; Rajamathi, C.R.; Rajamathi, M.; Gautam, U.K.; Wang, X.; Golberg, D.; Bando, Y. N-Doped Graphene—VO_2 (B) Nanosheet-Built 3D Flower Hybrid for Lithium Ion Battery. *ACS Appl. Mater. Interfaces* **2013**, *5*, 2708–2714. [CrossRef] [PubMed]
48. Kim, M.I.; Shim, J.; Li, T.; Lee, J.; Park, H.G. Fabrication of Nanoporous Nanocomposites Entrapping Fe_3O_4 Magnetic Nanoparticles and Oxidases for Colorimetric Biosensing. *Chem. Eur. J.* **2011**, *17*, 10700–10707. [CrossRef] [PubMed]
49. Edgar, P.; Yona, K. A Simple Colorimetric Method for the Measurement of Hydrogen Peroxide Produced by Cells in Culture. *J. Immunol. Methods* **1980**, *38*, 161–170.
50. Chen, X.; Zhou, X.D.; Hu, J. Pt-DNA complexes as peroxidase mimetics and their applications in colorimetric detection of H_2O_2 and glucose. *Anal. Methods* **2012**, *4*, 2183–2187. [CrossRef]